

**CRACK POINT STRESS SINGULARITIES
AT A BI-MATERIAL INTERFACE**

A. R. Zak
M. L. Williams

January 1962

This work was supported by the
National Aeronautics and Space Administration
Research Grant No. NsG-172-60: GALCIT 120

Graduate Aeronautical Laboratories
California Institute of Technology
Pasadena, California

ABSTRACT

A continuing study of plane stress singularities at corners and cracks has been extended to the case of a crack in a hard (soft) material ending normal to a continuous interface with a soft (hard) material. The increase (decrease) in stress singularity over the homogeneous material case, which is of the characteristic inverse square root of distance from the crack point, is given for all relative rigidities between zero and infinity. Associated changes in the principal stress and distortion strain energy density distribution are also discussed, along with indications of application to such situations as microcrack growth near grain boundaries and earth faults in layered strata.

CRACK POINT STRESS SINGULARITIES AT A BI-MATERIAL INTERFACE

Introduction

Continuing a series of papers devoted to the study of stress distributions in the vicinity of angular notches in sheet specimens subjected to plane stress, the present results deal with a particular limit case of a closed notch or line crack. Elastic analysis when applied to brittle fracture has generally been restricted to isotropic homogeneous media and based upon the initial work of Inglis and Griffith. The type solutions exploited in these recent investigations have also been found to apply to this isotropic homogeneous case for both bending (1, 2)* and extension^(3, 4). In addition certain limited results have been obtained for the case of a radial crack in sheet with polar orthotropy⁽⁵⁾. Finally a non-homogeneous application dealing with a crack occurring along a line separating two strata of different isotropic properties was studied, initially due to its geophysical application.⁽⁶⁾

This latter problem may also be interpreted, with some license, as related to the conditions at the point of a micro-crack along the grain boundary in a bi-material matrix. In this sense there is a companion problem, dealt with in this paper, which concerns the situation wherein a plane crack in one isotropic medium is on the verge of entering a different material. The general problem is of course that of the crack oriented at an arbitrary angle to the (grain) boundary but, while it can be treated in the same fashion, only the simpler problem of the crack oriented perpendicularly to the boundary between the two regions will be considered here.

Recalling that the strength of the elastic stress singularity for a stationary crack in an isotropic homogeneous medium is inversely proportional to the inverse square root of the distance from the crack point, the question to be investigated here is the character of the singular stress distribution as a crack is about to propagate from a harder to softer region, or vice versa.

*Refer to reference list in the back of the paper.

Outline of the Solution

The geometry of the crack in the two dissimilar media M_1 and M_2 is shown in Figure 1 below,

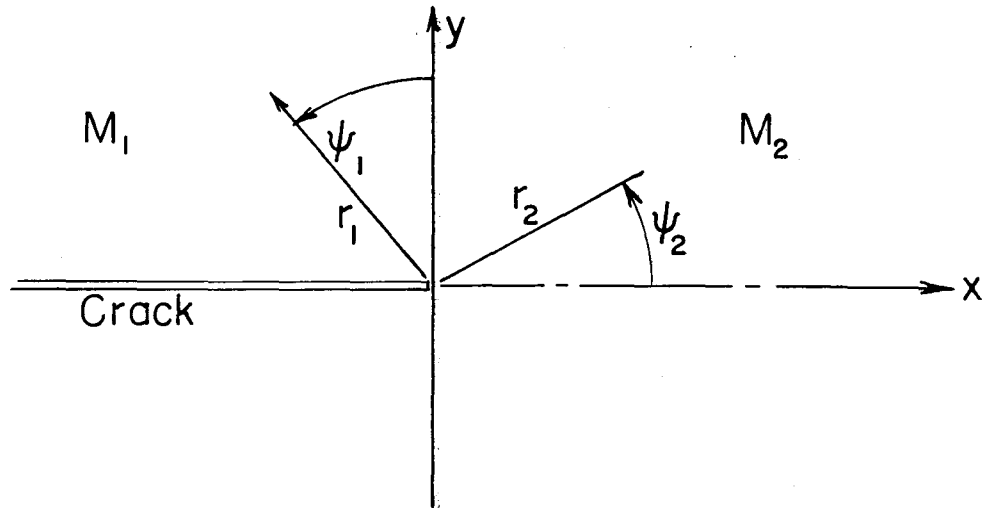


Figure 1.

The crack is assumed to exist in M_1 ($x < 0$). It terminates, and is perpendicular to the dividing line between the two media, $x = 0$. The method of solution for the stresses around the crack is the same as used in the previous investigations. A stress function $\chi(r, \psi)$ is found which satisfies the biharmonic equation

$$\nabla^4 \chi(r, \psi) \quad (1)$$

It must also be such that (a) the normal stress, σ_ψ , and the shear stress, $\tau_{r\psi}$, vanish along both sides of the crack, and (b) the normal stress σ_ψ , the shear stress $\tau_{r\psi}$, the radial displacement u_r , and the tangential displacement u_ψ are continuous across $x = 0$.

The general solution to (1) is chosen in the following form

$$\chi(r, \psi) = r^{\lambda+1} F(\psi) = r^{\lambda+1} [a \sin(\lambda+1)\psi + b \cos(\lambda+1)\psi + c \sin(\lambda-1)\psi + d \cos(\lambda-1)\psi] \quad (2)$$

where the relations between stresses, displacements, and the stress function are,

$$\sigma_r = \frac{1}{r^2} \frac{\partial^2 \chi}{\partial \psi^2} + \frac{1}{r} \frac{\partial \chi}{\partial r} = r^{\lambda-1} [F''(\psi) + (\lambda+1)F(\psi)] \quad (3)$$

$$\sigma_\psi = \frac{\partial^2 \chi}{\partial r^2} = r^{\lambda-1} \lambda(\lambda+1)F(\psi) \quad (4)$$

$$\tau_{r\psi} = -\frac{1}{r} \frac{\partial^2 \chi}{\partial r \partial \psi} + \frac{1}{r^2} \frac{\partial \chi}{\partial \psi} = -\lambda r^{\lambda-1} F'(\psi) \quad (5)$$

$$u_\psi = \frac{1}{2\mu} r^\lambda \left\{ -F'(\psi) - 4(1-\sigma)[c \cos(\lambda-1)\psi - d \sin(\lambda-1)\psi] \right\} \quad (6)$$

$$u_r = \frac{1}{2\mu} r^\lambda \left\{ -(\lambda+1)F(\psi) + 4(1-\sigma)[c \sin(\lambda-1)\psi + d \cos(\lambda-1)\psi] \right\} \quad (7)$$

In the above expressions μ is the shear modulus and $\sigma \equiv \frac{\nu}{1+\nu}$, where ν is the Poisson's ratio. The primes denote differentiation with respect to ψ .

Introducing a notation, let the quantities in regions M_1 and M_2 have the corresponding subscript, i. e. $F_1, F_2, \lambda_1, \lambda_2, \psi_1, \psi_2, a_1, a_2$ etc. For convenience the angle ψ_1 in M_1 is measured from the vertical and ψ_2 in M_2 from the horizontal, as shown in Figure 1. This will be understood in the subsequent analysis and the subscript will be dropped. Furthermore it will be found that $\lambda_1 = \lambda_2$ in order that the

radial variation of the continuity conditions on the demarcation line can be satisfied.

It is assumed in the present analysis that the media containing the crack is loaded symmetrically with respect to the crack. Therefore the stress function in the two media can be written in M_1 * as

$$F_1(\psi) = a_1 \sin(\lambda+1)\psi + b_1 \cos(\lambda+1)\psi + c_1 \sin(\lambda-1)\psi + d_1 \cos(\lambda-1)\psi \quad (8)$$

and in M_2 , upon taking advantage of the symmetry,

$$F_2(\psi) = b_2 \cos(\lambda+1)\psi + d_2 \cos(\lambda-1)\psi \quad (9)$$

The boundary conditions on the crack, $\sigma_\psi = 0$ and $\tau_{r\psi} = 0$, require

$$a_1 \sin(\lambda+1)\frac{\pi}{2} + b_1 \cos(\lambda+1)\frac{\pi}{2} + c_1 \sin(\lambda-1)\frac{\pi}{2} + d_1 \cos(\lambda-1)\frac{\pi}{2} = 0 \quad (10)$$

$$a_1(\lambda+1)\cos(\lambda+1)\frac{\pi}{2} - b_1(\lambda+1)\sin(\lambda+1)\frac{\pi}{2} + c_1(\lambda-1)\cos(\lambda-1)\frac{\pi}{2} - d_1(\lambda-1)\sin(\lambda-1)\frac{\pi}{2} = 0 \quad (11)$$

Matching the stresses σ_ψ and $\tau_{r\psi}$ in the two regions at the demarcation line leads to

$$b_1 + d_1 = b_2 \cos(\lambda+1)\frac{\pi}{2} + d_2 \cos(\lambda-1)\frac{\pi}{2} \quad (12)$$

* Strictly speaking, if Equation (8) is assumed to hold for M_1 above the crack then the stress function for M_1 below the crack will have the form $F_1(\psi) = -a_1 \sin(\lambda+1)\psi + b_1 \cos(\lambda+1)\psi - c_1 \sin(\lambda-1)\psi + d_1 \cos(\lambda-1)\psi$ the coefficients a_1 , b_1 , c_1 , d_1 are equal to the ones in Equation (8).

$$a_1(\lambda+1) + c_1(\lambda-1) = -b_2(\lambda+1) \sin(\lambda+1) \frac{\pi}{2} - d_2(\lambda-1) \sin(\lambda-1) \frac{\pi}{2} \quad (13)$$

after employing the previously mentioned condition that $\lambda_1 = \lambda_2$, while matching the displacements u_r, u_ψ here gives

$$\begin{aligned} & \frac{1}{2\mu_1} \{ -(\lambda+1)(b_1 + d_1) + 4(1-\sigma_1)d_1 \} \\ & = \frac{1}{2\mu_2} \{ -(\lambda+1) [b_2 \cos(\lambda+1) \frac{\pi}{2} + d_2 \cos(\lambda-1) \frac{\pi}{2}] + 4(1-\sigma_2) [d_2 \cos(\lambda-1) \frac{\pi}{2}] \} \end{aligned} \quad (14)$$

$$\begin{aligned} & \frac{1}{2\mu_1} \{ -(\lambda+1)a_1 - (\lambda-1)c_1 - 4(1-\sigma_1)c_1 \} \\ & = \frac{1}{2\mu_2} \{ (\lambda+1)b_2 \sin(\lambda+1) \frac{\pi}{2} + (\lambda-1)d_2 \sin(\lambda-1) \frac{\pi}{2} + 4(1-\sigma_2)d_2 \sin(\lambda-1) \frac{\pi}{2} \} \end{aligned} \quad (15)$$

Equations (10) to (15) are six linear, homogeneous equations in the unknown constants and for a non-trivial solution to exist the determinant of the coefficients of these six equations has to vanish. This determinant can easily be evaluated and put in the form

$$\begin{aligned} & [\lambda^2(-4\lambda^2 + 4\lambda\beta) + 2\lambda^2 - 2\lambda\beta + 2\lambda - \beta + 1] \sin \lambda \pi \\ & + [-2\lambda^2 + 2\lambda\beta - 2\lambda + 2\beta] \sin \lambda \pi \cos \lambda \pi = 0 \end{aligned} \quad (16)$$

where the notation

$$\lambda = \frac{k-1}{4(1-\sigma_1)}, \quad \beta = \frac{1-\sigma_2}{1-\sigma_1} k, \quad \text{and} \quad k = \frac{\mu_1}{\mu_2} \quad (17)$$

has been introduced.

For the special case, $\sigma_1 = \sigma_2$ and $k = 0$, $k = 1$ and $k = \infty$, corresponding to clamped-free (90 degree angle) free-free (360 degree angle) and free-free (90 degree angle) situations respectively, the characteristic values deduced from the equations given in Reference (3) can easily be obtained. In general, each combination of material properties, as reflected by the values of α and β in (17) will yield a set of eigenvalues of λ , which then define possible solutions for the stress function $\chi(r, \psi)$, within an arbitrary multiplicative constant, by solving for five of the unknowns in terms of the sixth in (10) - (15).

One possible solution to (16) is given by

$$\sin \lambda \tilde{\pi} = 0$$

corresponding to the eigenvalues $\lambda = 0, 1, 2, \dots$. The solution $\lambda = 0$ generates stresses which are identically equal to zero in the whole region and the remaining solutions $\lambda = 1, 2, \dots$ will not produce a stress singularity at the crack tip, while negative values leading to infinite displacements are not physically admissible.

The other possible solutions to (16) result from solving

$$A\lambda^2 + B + C \cos \lambda \tilde{\pi} = 0 \quad (18)$$

where

$$A = -4\alpha^2 + 4\alpha\beta$$

$$B = 2\alpha^2 - 2\alpha\beta + 2\alpha - \beta + 1$$

and

$$C = -2\alpha^2 + 2\alpha\beta - 2\alpha + 2\beta$$

In general λ will be complex and therefore will be written

$\lambda = x + iy$. Substituting into (18) and dividing the equation into real and imaginary parts, the following two equations are obtained

$$(x^2 - y^2)A + B + C \cos x\pi \cosh y\pi = 0 \quad (19)$$

$$2xyA - C \sin x\pi \sinh y\pi = 0 \quad (20)$$

When λ is real, Equation (9) will apply, viz.

$$x^2 A + B + C \cos x\pi = 0 \quad (21)$$

which can easily be solved graphically or numerically.

If λ is complex, write (19) and (20) in the form

$$\cos x\pi = - \frac{(x^2 - y^2)A + B}{C \cosh y\pi} \quad (22)$$

$$\sin x\pi = \frac{2xyA}{C \sinh y\pi} \quad (23)$$

and upon squaring (22) and (23) and adding, an equation is obtained which gives a solution of x in terms of y . Substituting for x into (19) or (20) then gives an equation in y only. This equation again has to be solved graphically or numerically, where it may be noted incidentally that the roots are infinite in number and ordered at infinity as found in a similar case investigated earlier⁽⁷⁾.

Since the purpose of this paper is to investigate stresses in the immediate neighborhood of the crack tip we are only interested in the smallest positive values of the real part of λ , which correspond to the strongest singularity. It happens that such values of λ come from the solution of Equation (21), that is when λ is real.

Discussion

As a first point of interest, the strength of the stress singularity is calculated for a range of values of k , assuming for simplicity that $\sigma_1 = \sigma_2$, i. e. equal to Poisson's ratio. The results of this calculation are shown in Figure 2, where λ is plotted against k . As the stresses at the crack tip, (3) - (5) are proportional to $r^{\lambda-1}$, it can be seen from Figure 2 that the strength of singularity increases as k increases, that is as the region M_2 ahead of the crack becomes "softer" with respect to M_1 , and vice versa. Furthermore, it can be shown that as $k \rightarrow \infty$, $\lambda \rightarrow 0$. In fact for large k the asymptotic expression is $\lambda = 0.881 (\mu_2 / \mu_1)^{1/2}$. It may be reiterated that for the limit $k = \infty$, the corresponding value of $\lambda = 0$ leads to the condition that the stresses vanish in the whole region.

Second, and in order to compare the characteristics of the stress variation when the crack proceeds from the soft to hard regions, and vice versa, the principal stresses around the crack tip have been computed and presented in Figure 3 for two values of the modulus ratio, $k = 1/20$ and $k = 20$. For comparison, the results for $k = 1$, from Reference (4) are also included in Figure 3.

The principal stresses near the crack point can be computed from the relations

$$\sigma_1 = \frac{\sigma_r + \sigma_\psi}{2} + \sqrt{\frac{(\sigma_r - \sigma_\psi)^2}{4} + \tau_{r\psi}^2} \quad (24)$$

$$\sigma_2 = \frac{\sigma_r + \sigma_\psi}{2} - \sqrt{\frac{(\sigma_r - \sigma_\psi)^2}{4} + \tau_{r\psi}^2} \quad (25)$$

where the stresses σ_r , σ_ψ , and $\tau_{r\psi}$ are calculated from, and correspond to, the value of λ which generates the singularity.

For $k = 1/20$ the minimum eigenvalue is $\lambda = 0.725$, (Figure 2). Using this value of λ the coefficients in (8) and (9) can be evaluated in

terms of d_2 , which for the present purpose can be taken as unity.

This step yields, *

$$F_1(\psi) = -0.1671 \sin 1.725\psi + 0.2579 \cos 1.725\psi \quad (26)$$

$$-0.1202 \sin 0.275\psi + 0.391 \cos 0.275\psi$$

and

$$F_2(\psi) = 0.2851 \cos 1.725\psi + \cos 0.275\psi \quad (27)$$

* The general expression for $F_1(\psi)$ and $F_2(\psi)$ are,

$$\begin{aligned} F_1(\psi) = & d_2 \left\{ \left[\frac{(3\lambda-1)\alpha + (1-2\lambda)\beta + \lambda}{(\lambda+1)(\lambda+1)} \right] [(\lambda-1) - 1] - \frac{\lambda-1}{\lambda+1} [(\lambda-1)\alpha + \beta - 1] \right\} \cos \lambda \frac{\pi}{2} \sin (\lambda+1)\psi \\ & + d_2 \left\{ \left[\frac{(3\lambda-1)\alpha + (1-2\lambda)\beta + \lambda}{(\lambda+1)(\lambda+1)} \right] [-(\lambda+1)\alpha - 1] + [(\lambda+1)\alpha - \beta + 1] \right\} \sin \lambda \frac{\pi}{2} \cos (\lambda+1)\psi \\ & + d_2 \left\{ \left[\frac{(3\lambda-1)\alpha + (1-2\lambda)\beta + \lambda}{(\lambda+1)(\lambda+1)} \right] [-(\lambda+1)\alpha] + [(\lambda-1)\alpha + \beta] \right\} \cos \lambda \frac{\pi}{2} \sin (\lambda-1)\psi \\ & + d_2 \left\{ \left[\frac{(3\lambda-1)\alpha + (1-2\lambda)\beta + \lambda}{(\lambda+1)(\lambda+1)} \right] [(\lambda+1)\alpha] + [-(\lambda+1)\alpha + \beta] \right\} \sin \lambda \frac{\pi}{2} \cos (\lambda-1)\psi \end{aligned}$$

$$F_2(\psi) = d_2 \left[\frac{(3\lambda-1)\alpha + (1-2\lambda)\beta + \lambda}{(\lambda+1)(\lambda+1)} \right] \cos (\lambda+1)\alpha + d_2 \cos (\lambda-1)\psi$$

For $k = 20$, $\lambda_{\min} = 0.185$, similar computations gives

$$F_1(\psi) = 2.38 \sin 1.185\psi - 6.159 \cos 1.185\psi - 6.06 \sin 0.815\psi + 6.107 \cos 0.815\psi \quad (28)$$

and

$$F_2(\psi) = 1.18 \cos 1.185\psi + \cos 0.815\psi \quad (29)$$

By the use of Equations (26) to (20) the stresses σ_r , σ_ψ , and $\tau_{r\psi}$ can be calculated in the vicinity of the crack point and subsequently, using (24) and (25) the principal stresses are obtained.

Finally the distortional strain energy density distribution has been calculated and presented in Figure 4, for the same range of modulus ratio. The expression for the distortional strain energy is

$$W_d = \frac{1}{12\mu} \left[(\sigma_1 - \sigma_2)^2 + (\sigma_2 - \sigma_3)^2 + (\sigma_3 - \sigma_1)^2 \right] \quad (30)$$

with $\sigma_3 = 0$ for this assumed case of plane stress.

The angle ψ in Figures 3 and 4 is taken to be continuous throughout the two regions M_1 and M_2 and is measured from the horizontal, as shown. In order to compare the stress distributions for the homogeneous case $k = 1$ with the results for $k = 1/20$ and $k = 20$, the normalizing coefficient a_1 in Reference 4 was associated with $-d_2$, both of which multiply the term $\cos(\lambda - 1)\psi$. Only the distribution can be compared for different values of k ; any quantitative conclusion from the results of Figures 3 and 4 would have no meaning because even under a fixed load the value of the coefficient d_2 would be different for different values of the parameter k .

In the homogeneous case, the maximum of the principal stress was found to occur ahead of the crack at \dagger 60 degrees to the direction of prolongation. This same tendency also is seen to prevail when the crack is in the softer of the two materials, even to the angular position. On the other hand when the crack is proceeding from the hard into the softer material, the maximum stress occurs along the interface and is nearly an order of magnitude larger than the largest principal stress ahead of the crack. Also, it was found in the homogeneous case that the principal stresses near the crack point along $\Psi = 0$ were equal, thus leading to a state of "two-dimensional" hydrostatic tension and consequently less yielding. For the non-homogeneous situation, the stresses differ, actually being

$$\frac{\sigma_r(r, 0)}{\sigma_\psi(r, 0)} = \frac{\frac{4 + 2\left(\frac{M_1}{M_2} - 1\right)(1 + \nu_1)}{\frac{E_1}{E_2}(1 - \nu_2) - (1 - \nu_1)} + (2\lambda - 1)}{\frac{4}{\frac{E_1}{E_2}(1 - \nu_2) - (1 - \nu_1)} - (2\lambda - 1)}$$

which is seen to approach unity when $M_1 \rightarrow M_2$. Presumably therefore, a larger plastic region at the crack tip might be expected.

Turning to the distribution of distortion energy, which has a maximum at approximately \dagger 70 degrees for the $k = 1$ case, it is seen that similar behavior to the principal stress variation is found. For $k = 1/20$, the maximum occurs ahead and to the sides of a crack entering a hard region, whereas, if entering a softer medium the maximum occurs at the interface.

The similarity in behavior of these two quantities seems to coincide with physical experience, with the latter situation leading toward a sort of peeling away of the softer material perpendicular to the crack direction. On the other hand it should be observed that there is a small range of rigidity ratios for which the maximum stress at the interface ($\Psi = \pi/2$) is still less than the absolute maximum at $\Psi = 60$ degrees.

In conclusion two brief remarks are in order: (1) the stress distributions have been arbitrarily limited to symmetrical loadings, and (2) the lowest eigen value for this example is real and thus gives strictly a monotonic decay of stress, $\sigma \sim r^{-a}$. This latter behavior is characteristically different than the associated case when the crack lies along the interface. Here the lowest eigen value is complex, and leads to a damped, trigonometric variation, viz

$\sigma \sim r^{-a} \cos (b \log r)$. It seems reasonable therefore to assume that at some intermediate inclination of the crack to the interface, the characteristic behavior will switch from one to the other, as controlled by the relative value of the smallest positive real part of the complex eigenvalue to the real root.

BIBLIOGRAPHY

1. Williams, M. L.: "Surface Stress Singularities Resulting from Various Boundary Conditions in Angular Corners of Plates Under Bending." Proc. First Nat. Cong. Applied Mechanics, June 1951.
2. Williams, M. L.; Owans, R. H.: "Stress Singularities in Angular Corners of Plates Having Linear Flexural Rigidities for Various Boundary Conditions." Proc. Second Nat. Cong. Applied Mechanics, June 1954.
3. Williams, M. L.: "Stress Singularities Resulting from Various Boundary Conditions in Angular Corners of Plates in Extension." Journal of Applied Mechanics, Trans. ASME Vol. 74, 1952, p. 526. See also: Discussion JAM, Vol. 20, No. 4, Dec. 1953, p. 590.
4. Williams, M. L.: "On the Stress Distribution at the Base of a Stationary Crack." Journal of Applied Mechanics, March 1956.
5. Chapkis, R. L.; Williams, M. L.: "Stress Singularities For a Sharp-Notched Polarly Orthotropic Plate." Proc. Third Nat. Cong. Applied Mechanics, June 1958.
6. Williams, M. L.: "The Stresses Around a Fault or Crack in Dissimilar Media." Bulletin of the Seismological Society of America, Vol. 49, No. 2, April 1959, 11. 199 - 204.
7. Williams, M. L.: "Theoretical and Experimental Effect of Sweep Upon the Stresses and Reflection Distribution in Aircraft Wings of High Solidity. Part 6 - The Plate Problem for a Cantilever Sector of Uniform Thickness." AFTR, No. 5761, November 1950.

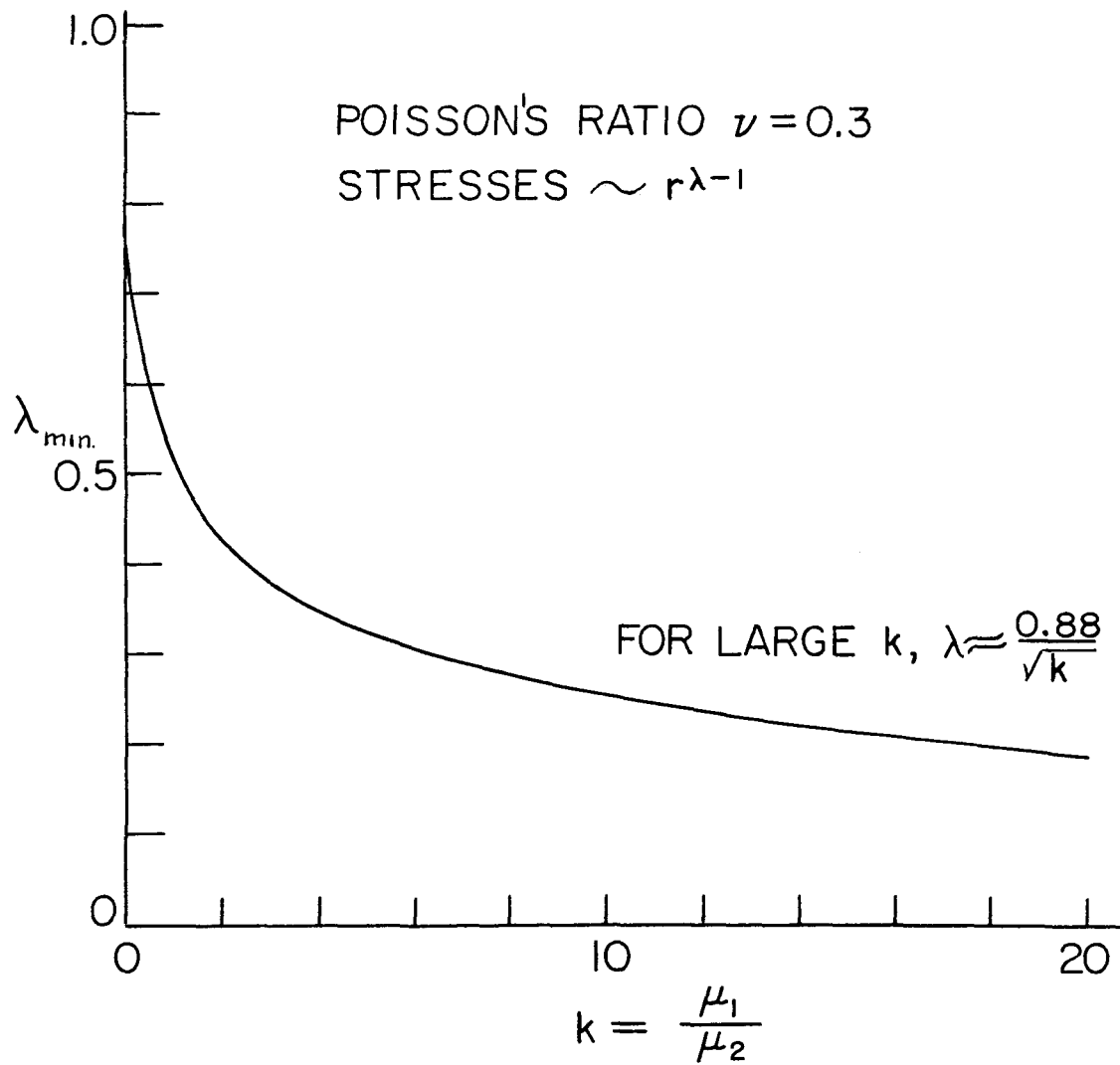


FIGURE 2. MINIMUM EIGENVALUE

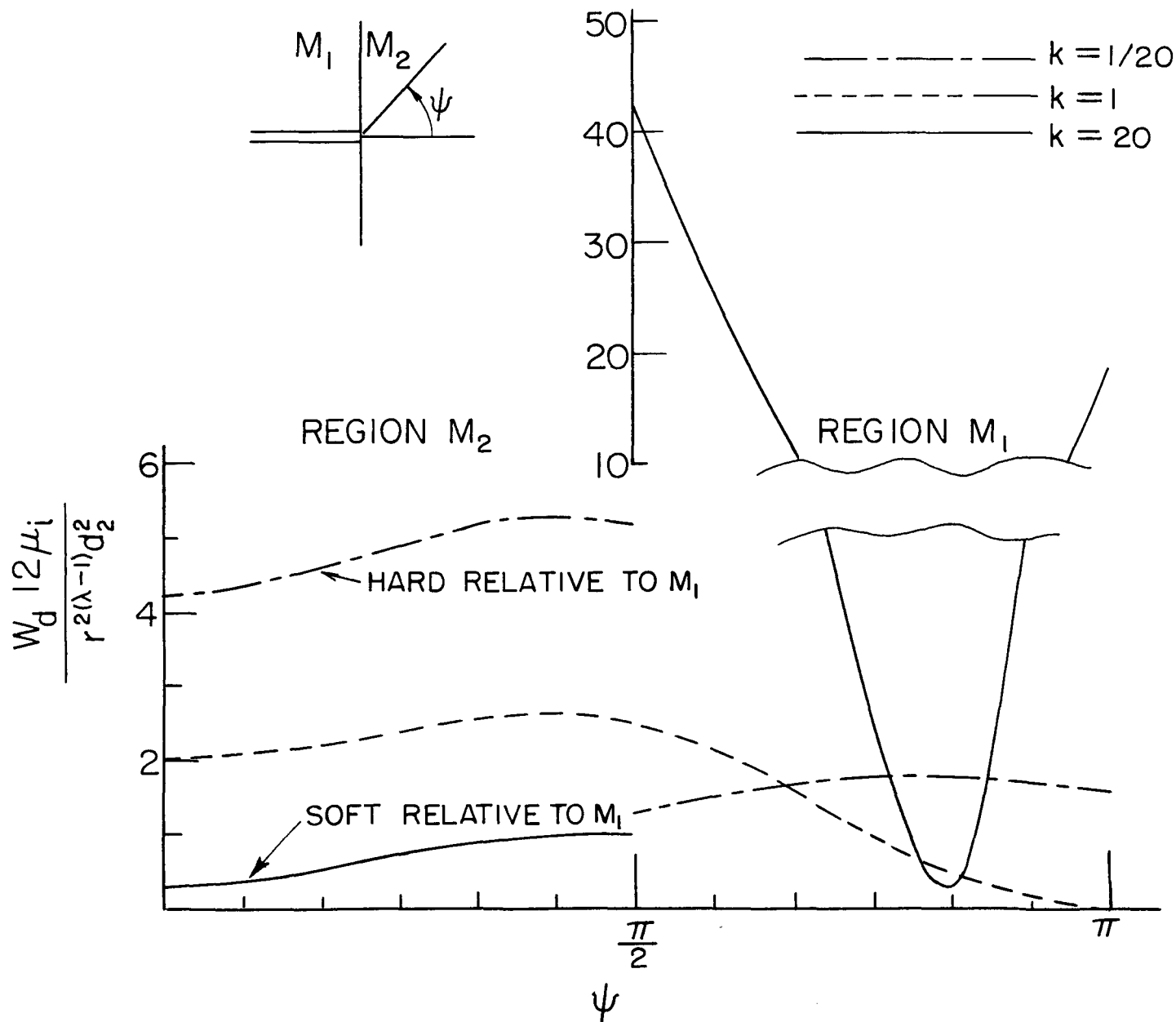


FIGURE 4. DISTORTION STRAIN ENERGY DISTRIBUTION

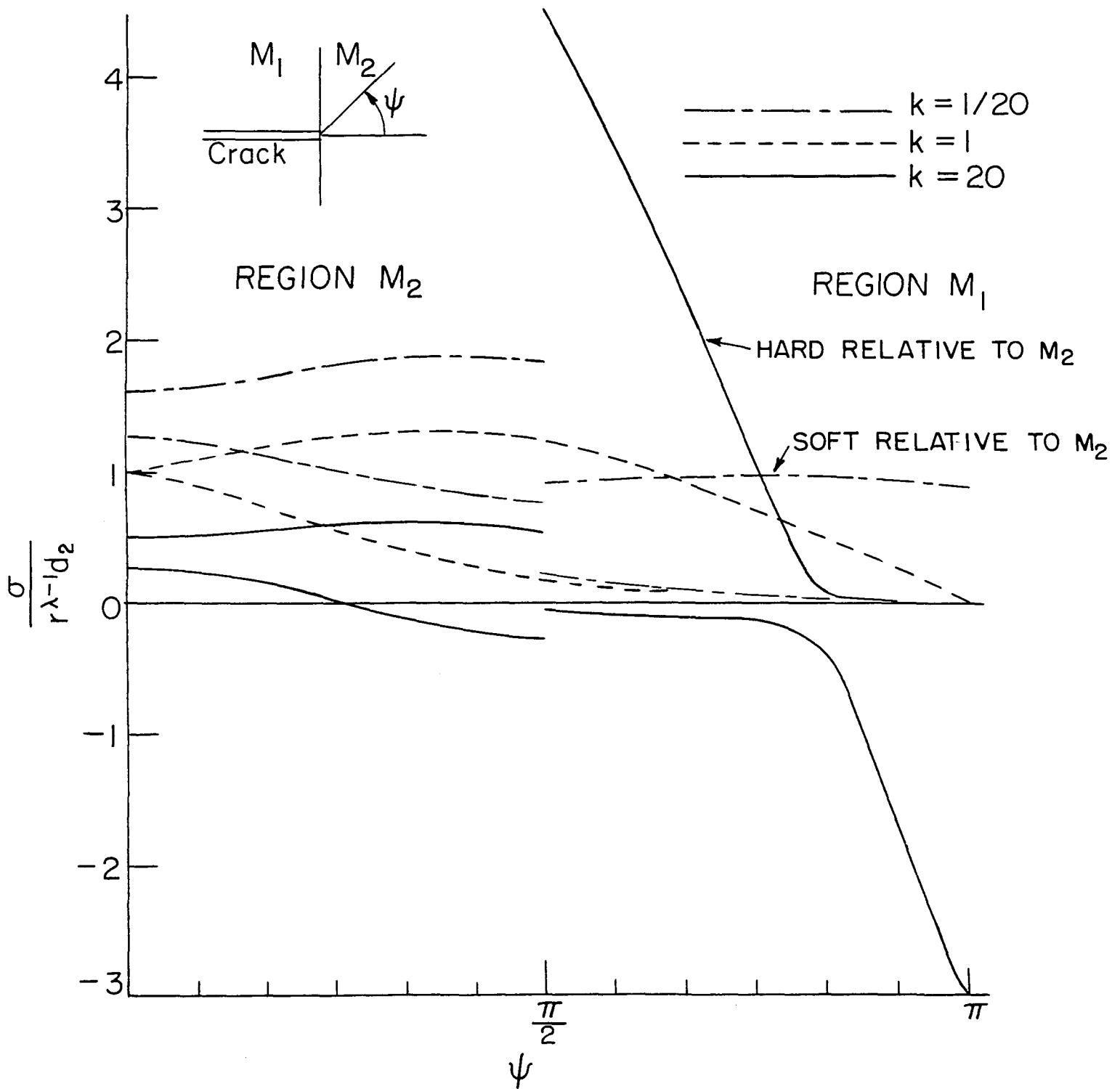


FIGURE 3. PRINCIPAL STRESS DISTRIBUTION

